International Journal of Research and Review
[Indexed, Peer-Reviewed Journal]
Volume 13; Issue: 6; June 2026
Website: www.ijrrjournal.com
Research Paper *E-ISSN: 2349-9788; P-ISSN: 2454-2237*

Electronic Structure and Thermoelectric Properties of Ni-Doped SnSe: A Density Functional Theory Study

Erik Bhekti Yutomo[1], Muhamad Fahmi[2]

[1,2]Department of Physics, Faculty of Science and Mathematics, Diponegoro University, Semarang, 50275, Indonesia.

Corresponding Author: Erik Bhekti Yutomo

DOI: https://doi.org/10.52403/ijrr.20260613

ABSTRACT

SnSe is a promising thermoelectric material owing to its low thermal conductivity and excellent energy conversion capability. In this study, the effect of Ni doping on the electronic and thermoelectric properties of SnSe was investigated using density functional theory (DFT) combined with Boltzmann transport theory. Structural optimization showed that Ni incorporation slightly contracts the lattice while preserving the orthorhombic crystal symmetry. Electronic structure calculations revealed that pristine SnSe exhibits an indirect band gap of 0.566 eV (unit cell) and 0.496 eV (supercell), whereas Ni doping introduces electronic states near the Fermi level and eliminates the band gap, resulting in metallic-like behavior. Projected density of states analysis confirmed that Ni-3d orbitals are responsible for the emergence of these states. Thermoelectric calculations at 300 K showed that Ni doping significantly increases electrical conductivity but reduces the Seebeck coefficient from 9.74×10^{-4} V/K to 4.61×10^{-4} V/K. Consequently, the power factor decreases compared to pristine SnSe. These results indicate that Ni doping effectively enhances electrical conductivity but is unfavorable for improving the thermoelectric performance of SnSe.

Keywords: SnSe, Ni doping, thermoelectric properties, density functional theory, electronic structure

INTRODUCTION

Climate change has become one of the most pressing global challenges, prompting countries worldwide to seek effective strategies for reducing greenhouse gas emissions and achieve sustainable development. Among various mitigation approaches, the deployment of renewable energy technologies has emerged as one of the most widely adopted solutions (1). Renewable energy sources, particularly solar and wind power, have experienced rapid growth in electricity generation over the past decade. The contribution of renewable energy to global electricity production is projected to continue increasing, reflecting the ongoing transition toward cleaner and more sustainable energy systems (2–4). This trend clearly demonstrates the growing commitment of countries worldwide to reducing dependence on fossil fuels and mitigating the impacts of climate change.

Among the various renewable energy technologies, thermoelectric energy conversion has attracted considerable attention because of its ability to directly convert thermal energy into electrical energy without moving parts.

Thermoelectric devices have demonstrated strong potential for applications in power generation, refrigeration, and sensing technologies (5). Thermoelectric materials can directly harvest waste heat and solar thermal energy, making them important components in the development of sustainable energy technologies. Compared with other energy-conversion systems, thermoelectric devices offer several advantages, including high reliability, long operational lifetime, compact design, and silent operation (6).

The performance of a thermoelectric material is commonly evaluated by the dimensionless figure of merit, $ZT = S^2\sigma T(\kappa_e + \kappa_l)^{-1}$, where T, κ_e, and κ_l represent the absolute temperature, electronic thermal conductivity, and lattice thermal conductivity, respectively (7). The parameters S and σ denote the Seebeck coefficient and electrical conductivity. Their combination, known as the power factor ($PF = (S^2\backslash\sigma)$, reflects the electronic transport performance of a thermoelectric material and plays a critical role in determining its overall efficiency.

Tin selenide (SnSe) has emerged as one of the most promising thermoelectric materials owing to its environmentally friendly, lead-free composition and outstanding thermoelectric performance. SnSe belongs to the family of layered group-IV monochalcogenides and exhibits a distorted rock-salt crystal structure with a temperature-dependent phase transition occurring at approximately 807 K (8,9). Experimental studies have revealed an ultralow lattice thermal conductivity of approximately 0.23 $W.m^{-}1.K^{-1}$, resulting in an exceptionally high ZT value of about 2.6 at 923 K along the crystallographic b-axis (10). Despite these remarkable properties, the practical application of SnSe remains limited by its relatively poor thermoelectric performance at low and intermediate temperatures, as well as concerns regarding long-term material stability (11).

To address these limitations, numerous studies have explored elemental doping as an effective strategy for improving the electronic transport properties of SnSe. Kim et al. (12) reported that Pb doping produced only a minor improvement in the power factor because the slight increase in the Seebeck coefficient was offset by a reduction in electrical conductivity. In contrast, Yuan et al. (13) demonstrated that Yb doping significantly enhanced the power factor, with $Sn_{0.98}Yb_{0.02}Se$ achieving a value of 0.78 $mW.m^{-1}.K^{-2}$ at 823 K, approximately 1.6 times higher than that of pristine SnSe. Furthermore, Al Bouzieh et al. (14) found that Bi/Zn co-doping produced substantially higher power factors than either pristine or singly doped SnSe, indicating that multi-element doping can effectively optimize the electronic transport properties of the material.

Although previous studies have demonstrated the effectiveness of doping strategies in enhancing the thermoelectric performance of SnSe, the achieved improvements remain insufficient for widespread commercial applications, particularly at lower operating temperatures. Therefore, the exploration of alternative dopants remains an important research direction. Transition metals are particularly attractive candidates because their partially filled d orbitals can significantly modify the electronic band structure, carrier concentration, and carrier transport behavior. Such modifications may provide new opportunities for optimizing the power factor and consequently improving the overall thermoelectric performance of SnSe.

In this work, the influence of Ni atom doping on the thermoelectric properties of SnSe is systematically investigated using first-principles calculations based on Density Functional Theory (DFT). DFT provides an accurate description of electron–ion interactions and enables reliable prediction of electronic properties that directly govern thermoelectric performance. By analyzing the effects of Ni dopants on the electronic structure and transport characteristics of SnSe, this study aims to identify promising doping strategies

for enhancing the power factor and improving thermoelectric efficiency at practical operating temperatures.

COMPUTATIONAL METHODOLOGY

First-principles calculations were performed within the framework of Density Functional Theory (DFT) using the Quantum ESPRESSO package (15). The exchange-correlation interaction was described by the Generalized Gradient Approximation (GGA) with the Perdew–Burke–Ernzerhof (PBE) functional (16), while the electron–ion interaction was treated using pseudopotentials. The crystal structure of pristine SnSe was adopted from the experimental work of Okazaki (17). SnSe crystallizes in an orthorhombic structure with lattice parameters of a = 11.57 Å, b = 4.19 Å, and c = 4.46) Å. Three computational models were considered in this study, namely the SnSe unit cell (SnSe-UC), a 2 × 2 × 2 SnSe supercell (SnSe-SC), and Ni-doped SnSe (SnSe-Ni), which was generated by substituting one Sn atom in the supercell with a Ni atom. The supercell approach was employed to simulate a dilute doping concentration while preserving periodic boundary conditions. The corresponding structural models are presented in Figure 1.

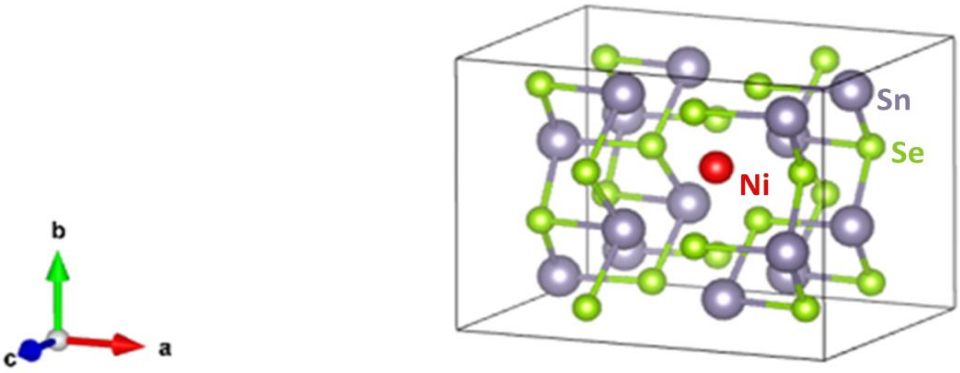

Figure 1. Crystal structure of Ni-doped SnSe (SnSe-Ni) constructed using a 2 × 2 × 2 supercell, where one Sn atom is substituted by a Ni atom.

Geometry optimization was performed for all models to obtain the minimum-energy configurations. Self-consistent field (SCF) calculations were subsequently carried out to determine the ground-state electronic density. The optimized structures were then used for non-self-consistent field (NSCF) calculations along the high-symmetry k-point path Γ–X–S–Y–Γ–Z–U–R–T–Z in the first Brillouin zone. Electronic band structures were obtained using the bands.x module and analyzed to determine the band gap characteristics as well as the influence of Ni doping on the electronic properties of SnSe.

To further investigate the electronic structure, the total density of states (DOS) and projected density of states (PDOS) were calculated using a denser k-point mesh than that employed in the SCF calculations. The DOS and PDOS analyses were performed using the projwfc.x utility to identify the contributions of Sn, Se, and Ni orbitals near the valence-band maximum and conduction-band minimum. These calculations provide insight into the electronic states responsible for charge transport and the modifications induced by Ni incorporation.

The thermoelectric transport properties were evaluated using the semiclassical Boltzmann transport theory within the constant relaxation time approximation as implemented in the BoltzTraP code (18). The electronic band energies obtained from DFT calculations were used as input for transport calculations. The Seebeck coefficient (S), electrical conductivity (σ), electronic thermal conductivity (κ_e), and power factor ($PF=S^2\sigma$) were calculated as functions of chemical potential and

temperature. The calculated transport properties were subsequently analyzed to evaluate the effect of Ni doping on the thermoelectric performance of SnSe and to identify the underlying electronic mechanisms responsible for the observed behavior.

RESULT AND DISCUSSION

The optimized lattice parameters of the SnSe unit cell (SnSe-UC), SnSe supercell (SnSe-SC), and Ni-doped SnSe (SnSe-Ni) are summarized in Table 1. For the pristine SnSe unit cell, the optimized structure preserves the orthorhombic symmetry with lattice angles of $\alpha = \beta = \gamma = 90°$, indicating that the geometry optimization successfully converged to a stable ground-state configuration. The obtained lattice parameters are in good agreement with previously reported experimental and theoretical values. Zhao et al. (10) reported lattice constants of a = 11.58 Å, b = 4.22 Å, and c = 4.40 Å for orthorhombic SnSe, while Rosnita et al. (19) obtained values of a = 11.49 Å, b = 4.44 Å, and c = 4.14 Å. The close agreement between the present results and previous studies confirms the reliability of the adopted computational approach.

Table 1. Optimized lattice parameters (a, b, and c) and lattice angles (α, β, and γ) of the pristine SnSe unit cell (SnSe-UC), SnSe supercell (SnSe-SC), and Ni-doped SnSe (SnSe-Ni).

Models	Lattice parameters	Lattice Angles
SnSe-UC	a = 11,44281Å b = 4,15665 Å c = 4,43729 Å	α = 90,000° β = 90,000° γ = 90,000°
SnSe-SC	a = 11.57100 Å b = 8.38800 Å c = 8.90514 Å	α = 90,000° β = 90,000° γ = 90,000°
SnSe-Ni	a = 11.46683 Å b = 8.27499 Å c = 8.77784 Å	α = 90,000° β = 90,000° γ = 90,000°

The SnSe supercell was constructed by expanding the optimized unit cell to provide a suitable framework for simulating dilute Ni doping. As expected, the lattice parameters increased proportionally according to the supercell dimensions while preserving the orthorhombic crystal symmetry. The absence of significant structural distortion indicates that the generated supercell remained geometrically stable after structural relaxation.

After substituting one Sn atom with a Ni atom, slight reductions in all lattice parameters were observed compared with the pristine supercell, as shown in Table 1. This lattice contraction can be attributed to the smaller atomic radius of Ni (~1.24 Å) relative to Sn (~1.45 Å). The incorporation of the smaller Ni atom into the Sn site leads to shorter bond lengths and a more compact crystal structure. Despite this contraction, the lattice angles remained unchanged at 90°, indicating that the orthorhombic symmetry was preserved after doping. The absence of significant structural deformation suggests that the Ni atom can be accommodated within the SnSe lattice without inducing substantial crystal instability. These results demonstrate that the Ni-doped structure is geometrically stable and suitable for subsequent electronic and thermoelectric analyses.

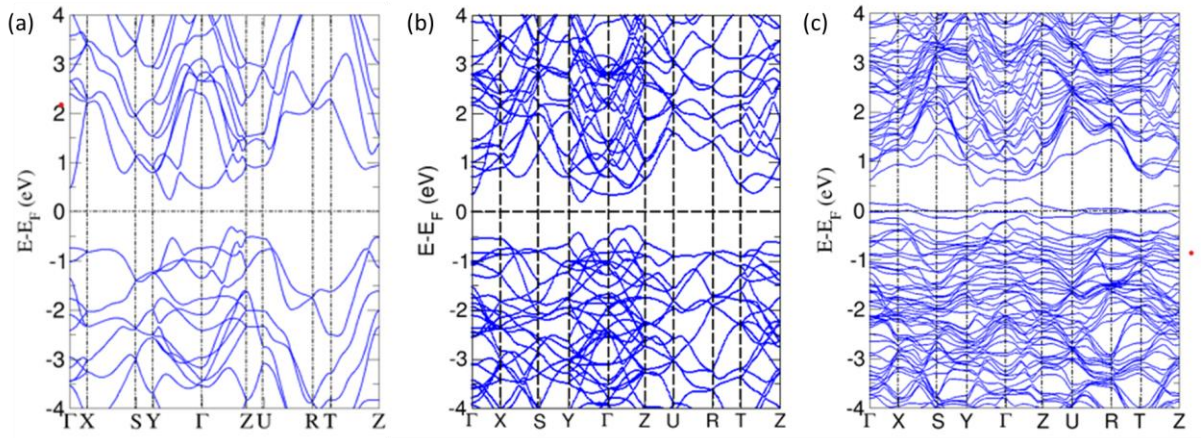

Figure 2. Calculated electronic band structures of (a) pristine SnSe unit cell (SnSe-UC), (b) SnSe supercell (SnSe-SC), and (c) Ni-doped SnSe (SnSe-Ni). The dashed horizontal line denotes the Fermi level (E_F=0 eV).

Following the structural analysis, the electronic properties of pristine and Ni-doped SnSe were investigated through band structure calculations. The calculated band structures of the SnSe unit cell (SnSe-UC), SnSe supercell (SnSe-SC), and Ni-doped SnSe (SnSe-Ni) are shown in Figure 2. As shown in Figure 2(a), the pristine SnSe unit cell exhibits an indirect-band-gap semiconducting character, with the valence band maximum (VBM) and conduction band minimum (CBM) located at different k-points. The calculated band gap is 0.566 eV, which is lower than the experimental value of approximately 0.86–0.90 eV. However, this result agrees well with previous GGA-PBE calculations, which reported band gaps in the range of 0.45–0.55 eV due to the well-known underestimation of band gaps in conventional DFT methods (20,21).

The electronic structure of the supercell, shown in Figure 2(b), remains similar to that of the unit cell. The calculated band gap decreases slightly to 0.496 eV while preserving the indirect-gap nature of SnSe. This minor reduction can be attributed to the band-folding effect associated with the enlarged supercell. The overall similarity between the UC and SC results indicates that the supercell construction does not significantly alter the intrinsic electronic properties of SnSe and is therefore suitable for doping studies.

A pronounced change is observed after Ni incorporation, as shown in Figure 2(c). The band gap disappears completely, and several bands cross the Fermi level, indicating a transition from semiconducting to metallic or semimetallic behavior. This change originates from the introduction of Ni 3d states near the Fermi level, which hybridize with the Sn and Se orbitals and generate additional electronic states within the original band-gap region. Similar band-gap suppression has been reported in previous studies of doped SnSe systems (22). Overall, the results demonstrate that while the supercell construction has only a minor effect on the electronic structure, Ni doping significantly modifies the band structure by introducing states at the Fermi level. Such changes are expected to influence the carrier transport behavior and thermoelectric performance of SnSe.

To further understand the origin of the electronic states observed in the band structure, the projected density of states (PDOS) of the SnSe unit cell (SnSe-UC), SnSe supercell (SnSe-SC), and Ni-doped SnSe (SnSe-Ni) were analyzed, as shown in Figure 3. For pristine SnSe, both the unit cell and supercell exhibit similar PDOS characteristics, confirming that the supercell construction does not significantly alter the intrinsic electronic structure of the material. As shown in Figures 3(a) and 3(b), the deep valence region between approximately –15

and –12 eV is mainly contributed by Se-4s orbitals, while the energy range from –8 to –6 eV is dominated by Sn-5s states with minor hybridization with Se orbitals. Near the valence band maximum (VBM), the electronic states are primarily composed of Se-4p orbitals with contributions from Sn-5p states, indicating strong p–p hybridization between Sn and Se atoms. The conduction band region above the Fermi level is therefore largely characterized by Sn-5p states, confirming that the electronic transition across the band gap mainly involves p–p orbital interactions.

A significant modification of the electronic structure occurs after Ni incorporation, as shown in Figure 3(c). New electronic states emerge in the energy range close to the Fermi level, originating predominantly from Ni-3d orbitals. Unlike pristine SnSe, the density of states at the Fermi level becomes nonzero, indicating the disappearance of the semiconducting gap and the emergence of metallic or semimetallic behavior. The presence of these states is consistent with the band structure results discussed previously, where several bands were found to cross the Fermi level. Furthermore, strong hybridization between Ni-3d and Sn/Se-p orbitals is observed in the energy range from approximately –3 to 0 eV. Such d–p hybridization is a common feature of transition-metal doping and plays a crucial role in modifying the electronic properties of chalcogenide materials.

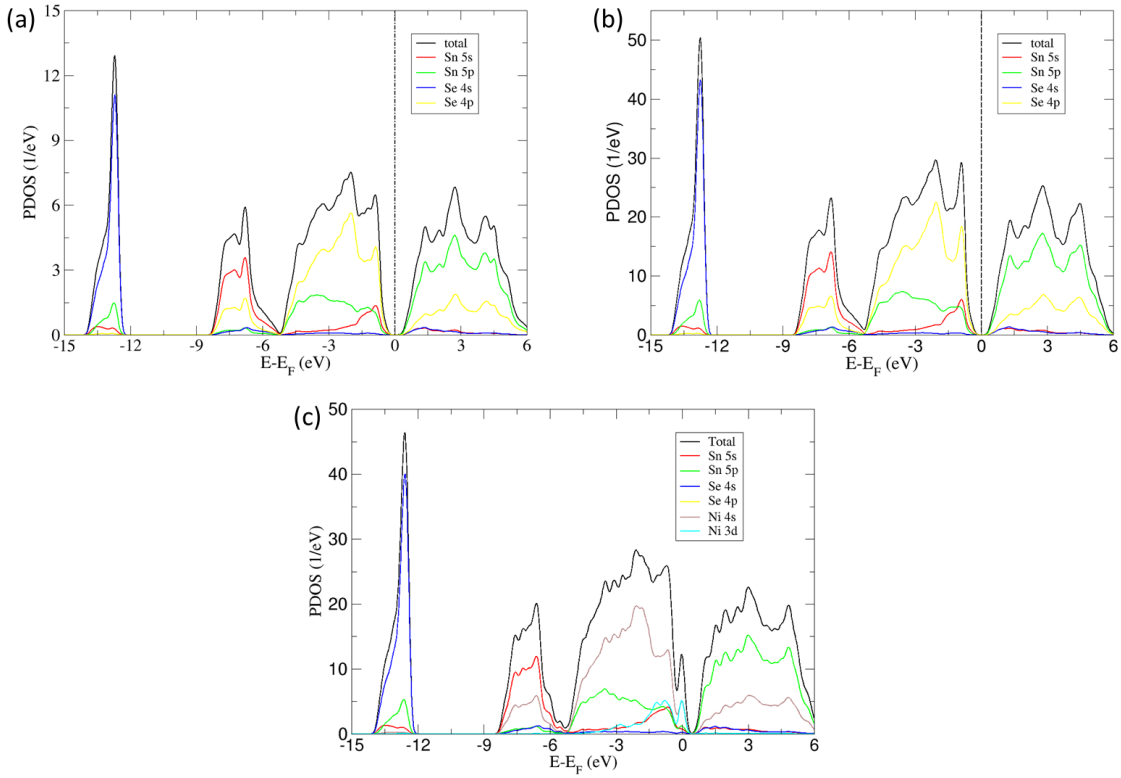

Figure 3. Projected density of states (PDOS) of (a) pristine SnSe unit cell (SnSe-UC), (b) pristine SnSe supercell (SnSe-SC), and (c) Ni-doped SnSe (SnSe-Ni). The vertical dashed line indicates the Fermi level (E_F=0 eV).

Overall, the PDOS analysis confirms that the electronic states introduced by Ni doping are responsible for the closure of the band gap and the increased density of states around the Fermi level. These changes are expected to enhance carrier concentration and electrical conductivity, which are important factors governing the thermoelectric performance of the material.

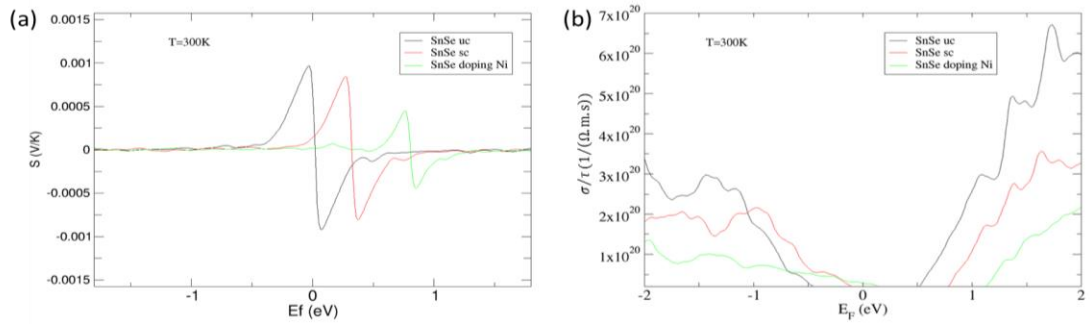

Figure 4. Thermoelectric transport properties of pristine and Ni-doped SnSe at 300 K: (a) Seebeck coefficient and (b) electrical conductivity as functions of Fermi energy.

The impact of Ni doping on the thermoelectric performance of SnSe was further evaluated through the Seebeck coefficient, electrical conductivity, and power factor at 300 K. The calculated Seebeck coefficient and electrical conductivity as functions of Fermi energy are presented in Figure 4, while the corresponding power factor is shown in Figure 5. As shown in Figure 4(a), pristine SnSe exhibits a relatively high Seebeck coefficient, with maximum values of 9.74×10^{-4} V/K and 8.57×10^{-4} V/K for the unit cell (UC) and supercell (SC), respectively. These high values are attributed to the semiconducting nature of SnSe, where the presence of a band gap produces a strong asymmetry in the electronic density of states around the Fermi level. The slight reduction observed in the supercell model indicates that the enlarged structure has a minor influence on the electronic distribution while preserving the intrinsic thermoelectric characteristics of SnSe. A different trend is observed after Ni incorporation. The maximum Seebeck coefficient decreases significantly to 4.61×10^{-4} V/K, nearly half that of pristine SnSe. This reduction is closely related to the appearance of Ni-derived electronic states near the Fermi level, as revealed by the band structure and PDOS analyses. The increased carrier concentration reduces the asymmetry of the electronic states around the Fermi level, resulting in a lower thermoelectric voltage generation capability. The electrical conductivity results shown in Figure 4(b) exhibit the opposite behavior. Pristine SnSe displays relatively low conductivity due to its semiconducting character and limited intrinsic carrier concentration. In contrast, Ni doping leads to a substantial increase in electrical conductivity, which can be attributed to the emergence of Ni-3d states crossing the Fermi level. These additional states provide more charge carriers and facilitate electronic transport, consistent with the transition from semiconducting to metallic-like behavior observed in the electronic structure calculations.

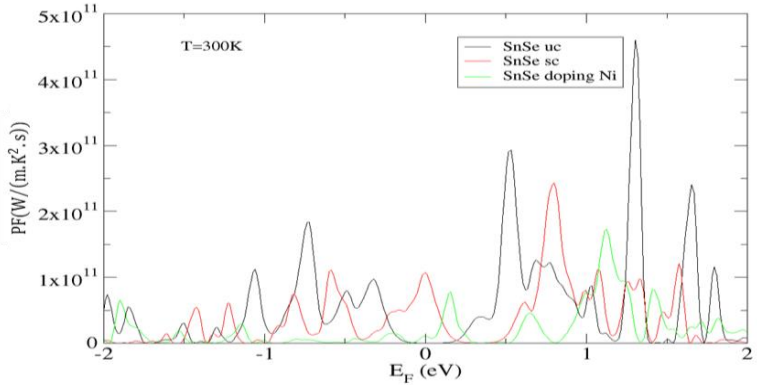

Figure 5. Power factor of pristine SnSe unit cell (SnSe-UC), pristine SnSe supercell (SnSe-SC), and Ni-doped SnSe (SnSe-Ni) as a function of Fermi energy at 300 K.

The combined effect of the Seebeck coefficient and electrical conductivity is reflected in the power factor (PF), presented in Figure 5. Although Ni doping significantly enhances electrical conductivity, the corresponding decrease in the Seebeck coefficient is more pronounced. As a result, the power factor of SnSe-Ni is lower than those of the pristine UC and SC systems. This behavior indicates that the improvement in carrier transport is insufficient to compensate for the loss of thermoelectric voltage generation capability. Overall, the thermoelectric analysis demonstrates that Ni doping effectively increases the electrical conductivity of SnSe by introducing additional electronic states near the Fermi level. However, the simultaneous reduction in the Seebeck coefficient leads to a lower power factor. These results suggest that Ni is more effective in enhancing the electrical conductivity than improving the thermoelectric performance of SnSe.

CONCLUSION

The effects of Ni doping on the electronic and thermoelectric properties of SnSe were investigated using DFT and Boltzmann transport calculations. The optimized structures remained stable and preserved the orthorhombic crystal symmetry after Ni incorporation. Pristine SnSe exhibited indirect-band-gap semiconducting behavior, whereas Ni doping introduced Ni-3d states near the Fermi level, leading to band-gap closure and metallic-like characteristics. As a result, electrical conductivity increased significantly, while the Seebeck coefficient decreased substantially. The reduction in the Seebeck coefficient dominated the overall thermoelectric response, resulting in a lower power factor. Therefore, although Ni doping enhances the electrical conductivity of SnSe, it is not an effective approach for improving its thermoelectric performance.

Declaration by Authors

Acknowledgement: None
Source of Funding: None
Conflict of Interest: The authors declare no conflict of interest.

REFERENCES

1. Maidasari T, Prakoso L Y, Murtiana S. Renewable energy as a green economy stimulus in Indonesia. Jurnal Energi Baru dan Terbarukan. 2023;4(3):183–191.
2. Dey P P, Das D C, Latif A, Hussain S M S, Ustun T S. Active power management of virtual power plant under penetration of central receiver solar thermal-wind using butterfly optimization technique. Sustainability. 2020;12(17):6979.
3. Abdolrasol M G M, Hannan M A, Hussain S M S, Ustun T S, Sarker M R, Ker P J. Energy management scheduling for microgrids in the virtual power plant system using artificial neural networks. Energies. 2021;14(20):6507.
4. Chauhan A, Upadhyay S, Khan M T, Hussain S M S, Ustun T S. Performance investigation of a solar photovoltaic/diesel generator based hybrid system with cycle charging strategy using BBO algorithm. Sustainability. 2021;13(14):8048.
5. Baghel N, Kumar A. Sustainable thermoelectric materials for solar energy applications: A review. Solid State Sciences. 2025; 160:107784.
6. Li D, Gong Y, Chen Y, Lin J, Khan Q, Zhang Y, Li Y, Zhang H, Xie H. Recent progress of two-dimensional thermoelectric materials. Nano-Micro Letters. 2020; 12:36.
7. Gusmao M S, Mota C, Ghosh A, Frota H O. Thermoelectric properties of SnSe (Pnma) under hydrostatic pressure. Computational Materials Science. 2018; 152:243–247.
8. Wei T R, Tan G, Zhang X, Wu C F, Li J F, Dravid V P, Snyder G J, Kanatzidis M G. Distinct impact of alkali-ion doping on electrical transport properties of thermoelectric p-type polycrystalline SnSe. Journal of The American Chemical Society. 2016;138(28):8875–8882.
9. Li Y, Shi X, Ren D, Chen J, Chen L. Investigation of the anisotropic thermoelectric properties of oriented polycrystalline SnSe. Energies. 2015;8(7):6275–6285.
10. Zhao L D, Lo S H, Zhang Y, Sun H, Tan G, Uher C, Wolverton C, Dravid V P, Kanatzidis M G. Ultralow thermal conductivity and high thermoelectric figure

of merit in SnSe crystals. Nature. 2014; 508:373–377.
11. Chen Z G, Shi X, Zhao L D, Zou J. High-performance SnSe thermoelectric materials: Progress and future challenge. Progress in Materias Science. 2018; 97:283–346.
12. Kim H S, Choi G, Ha M Y, Kim D H, Park S H, Chung I, Lee W B. Thermoelectric transport properties of Pb-doped SnSe alloys (PbxSn1−xSe): DFT-BTE simulations. Journal of Solid State Chemistry. 2019; 270:413–418.
13. Yuan J, Jin K, Shi Z, Fu L, Xu B. Enhanced thermoelectric performance of polycrystalline SnSe by doping with the heavy rare earth element Yb. Journal of Alloys and Compounds. 2022; 907:164438.
14. Al Bouzieh N, Benkraouda M, Amrane N. Electronic, Mechanical, and thermoelectric properties of Ge/Zn co-doped SnSe: first-principles calculations. Journal of Physics: Conference Series. 2024; 2751:012014.
15. Giannozzi P, Andreussi O, Brumme T, Bunau O, Nardelli M B, Calandra M, Car R, Cavazzoni C, Ceresoli D, Cococcioni M. Advanced capabilities for materials modelling with Quantum ESPRESSO. Journal of Physics: Condensed Matter. 2017;29(46):465901.
16. Perdew J P, Burke K, Ernzerhof M. Generalized gradient approximation made simple. Physical Review Letter. 1996;77(18):3865–3868.
17. Okazaki A, Ueda I. The crystal structure of stannous selenide SnSe. Journal of the Physical Society of Japan. 1956; 11:470.
18. Madsen G K H, Carrete J, Verstraete M J. BoltzTraP2, a program for interpolating band structures and calculating semi-classical transport coefficients. Computer Physics Communications. 2018; 231:140–145.
19. Rosnita M A, Fatima N, Mohamed R, Syafiq U, Ibrahim M A. An overview of the strategies for tin selenide advancement in thermoelectric application. Micromachines 2021;12;1463.
20. Kutorasinski K, Wiendlocha B, Kaprzyk S, Tobola J. Electronic structure and thermoelectric properties of n- and p-type SnSe from first-principles calculations. Physical Review B. 2015; 91:205201.
21. Zhou Y, Li W, Wu M, Zhao L D, He J, Wei S H, Huang L. Influence of defects on the thermoelectricity in SnSe: A comprehensive theoretical study. Physical Review B. 2018; 97:245202.
22. Echbani B, Bekkioui N, Brahim A A, Ez-Zahraouy H. DFT-based first-principles study of structural, electronic, optical, and photocatalytic properties of oxygen-doped SnSe. Computational Condensed Matter. 2026;46: e01183.

How to cite this article: Erik Bhekti Yutomo, Muhamad Fahmi. Electronic structure and thermoelectric properties of NI-doped SnSe: a density functional theory study. *International Journal of Research and Review*. 2026; 13(6): 128-136. DOI: *10.52403/ijrr.20260613*

******